Structural Conservation of Ligand Binding Reveals a Bile Acid-like Signaling Pathway in Nematodes*[S]

Xiaoyong Zhi[‡], X. Edward Zhou[‡], Karsten Melcher[‡§], Daniel L. Motola[¶1], Verena Gelmedin[||], John Hawdon[||], Steven A. Kliewer[¶**], David J. Mangelsdorf[¶‡‡], and H. Eric Xu[‡§2]

From the [‡]Laboratory of Structural Sciences and [§]Laboratory of Structural Biology and Biochemistry, Van Andel Research Institute, Grand Rapids, Michigan 49503, the Departments of [¶]Pharmacology and [**]Molecular Biology and [‡‡]Howard Hughes Medical Institute, University of Texas Southwestern Medical Center, Dallas, Texas 75390, the [||]Department of Microbiology, Immunology, and Tropical Medicine, George Washington University Medical Center, Washington, D. C. 20037, and the [§§]VARI-SIMM Center, Center for Structure and Function of Drug Targets, State Key Laboratory of Drug Research, Shanghai Institute of Materia Medica, Chinese Academy of Sciences, Shanghai 201203, China

Background: Nematode DAF-12s have species-specific ligand responses.
Results: Structures of a hookworm DAF-12 complexed with two different agonists are determined.
Conclusion: Bile acid-like signaling pathways have been conserved in mammals and nematodes.
Significance: Structural understanding of the hookworm DAF-12 activation is instrumental in treating nematode parasitism and points to the basis for evolution of a novel gut parasite hormone signaling pathway.

Bile acid-like molecules named dafachronic acids (DAs) control the dauer formation program in *Caenorhabditis elegans* through the nuclear receptor DAF-12. This mechanism is conserved in parasitic nematodes to regulate their dauer-like infective larval stage, and as such, the DAF-12 ligand binding domain has been identified as an important therapeutic target in human parasitic hookworm species that infect more than 600 million people worldwide. Here, we report two x-ray crystal structures of the hookworm *Ancylostoma ceylanicum* DAF-12 ligand binding domain in complex with DA and cholestenoic acid (a bile acid-like metabolite), respectively. Structure analysis and functional studies reveal key residues responsible for species-specific ligand responses of DAF-12. Furthermore, DA binds to DAF-12 mechanistically and is structurally similar to bile acids binding to the mammalian bile acid receptor farnesoid X receptor. Activation of DAF-12 by cholestenoic acid and the cholestenoic acid complex structure suggest that bile acid-like signaling pathways have been conserved in nematodes and mammals. Together, these results reveal the molecular mechanism for the interplay between parasite and host, provide a structural framework for DAF-12 as a promising target in treating nematode parasitism, and provide insight into the evolution of gut parasite hormone-signaling pathways.

DAs[3] are a group of bile acid-like steroid hormones that were first identified as endogenous ligands for DAF-12 in *Caenorhabditis elegans* (1). The position of the double bond on the steroid rings discriminates Δ4- and Δ7-dafachronic acids that both are synthesized *de novo* from cholesterol through several steps catalyzed by P450 enzymes, including DAF-36 and DAF-9 (2). DAF-9 catalyzes the last step of DA production by forming hydroxyl groups on the side acyl chain of its 3-keto substrates. It has been proposed that DAF-9 is the worm ortholog of mammalian CYP27A (1), a cytochrome P450 enzyme that catalyzes consecutive hydroxylations of substrate and acts at the late stage of bile acid production (3). DAF-36 is postulated to work at the earlier step of Δ7-DA production as a Rieske-like oxygenase, followed by the potential reductases and dehydrogenases to produce DA precursors (2, 4).

DAs control the dauer formation program in *C. elegans* through the nuclear receptor DAF-12 (1, 5). The dauer formation is an alternative developmental strategy that is adopted by the worms to tackle harsh environmental conditions. During dauer diapause, worms undergo significant changes in their morphology, physiology, metabolism, and behavior in comparison with the third larvae stage (L3) of their normal reproductive development (6, 7). The dauer formation program is transcriptionally regulated by the presence of DAs and their binding to the receptor DAF-12. In the absence of DAs, DAF-12 occupies the response elements within its promoters, recruits the corepressor DIN-1 to silence the expression of reproductive genes, and thus promotes entry into the dauer stage (8). In the presence of DAs, DAF-12 dissociates from corepressors and binds coactivators to activate a battery of genes that favor the reproductive growth and repress the dauer formation. The production of DAs is determined by DAF-9, which itself is under

[3] The abbreviations used are: DA, dafachronic acid; LBD, ligand binding domain; r.m.s.d., root mean square deviation; FXR, farnesoid X receptor; LXR, liver X receptor; 6ECDCA, 6α-ethyl-chenodeoxycholic acid; LCA, lithocholic acid.

the control of upstream signaling pathways (7). As such, signaling circuits initiated by responses to environmental changes converge at the DA production and DAF-12 activity to control the developmental choice (7).

Nematode parasitism is a threat to human health care and economic development (9). The hookworm species (including *Ancylostoma ceylanicum* and *Necator americanus* in this study) infect more than 600 million people worldwide (10). Parasitic nematodes are believed to have evolved from free-living ancestors, and their third larvae stage (infective, iL3) is morphologically similar to the dauer stage in *C. elegans* (11–13). Recent studies revealed the importance of the DAF-12 signaling in regulation of the iL3 in parasitic nematodes (14, 15). DAF-12 homologs in the threadworm *Strongyloides stercoralis* (*Sst*-DAF-12) and the hookworms *A. ceylanicum* (*Ace*DAF-12, panspecific), *Ancylostoma caninum* (*Aca*DAF-12, dog-specific), and *N. americanus* (*Nam*DAF-12, specific to humans) have been cloned, and sequence analysis reveals a significant level of identity with *C. elegans* DAF-12 (*Cel*DAF-12) (14). The LBDs of hookworm DAF-12s share 46% identity to the *Sst*DAF-12 LBD and 58% identity to the *Cel*DAF-12 LBD (see Fig. 1*A*). The parasitic DAF-12s can be activated by DAs in *in vitro* assays. Moreover, DA treatment partially caused their iL3 larvae to start feeding. (25S)-Δ7-DA effectively blocked iL3 formation in *S. stercoralis* by forcing the iL3 larvae to prematurely molt into development-defective larvae, thus markedly reducing the pathogenic iL3 population. These findings suggested that DAF-12 is a conserved nuclear receptor across nematode species and established DAF-12 as a potential drug target to treat nematode parasitism (14). Orthologs of the DA synthesis enzyme DAF-9 could not be identified in hookworms and threadworms (14). In addition, presumably because of the lack of a functional DAF-9, hookworm iL3 larvae could not be rescued in the presence of the DA precursor lathosterone, whereas *C. elegans* dauer larvae (*daf-36* mutants) could be rescued (2, 14). Currently it remains unknown how DAF-12 of parasitic nematodes is activated physiologically.

The crystal structure of the threadworm *Sst*DAF-12 LBD has been solved and revealed the general molecular basis for receptor activation in the presence of DAs. However, mutational studies indicated species-specific pharmacological responses (14). To further study the structural biology of DAF-12 and to elucidate the structural basis for species-specific ligand binding, we solved the crystal structure of the hookworm *Ace*DAF-12 LBD bound to (25S)-Δ7-DA. By comparing the two parasitic DAF-12 LBD structures, we identified the structural elements responsible for the species-specific ligand responses. Furthermore, we compared the *Ace*DAF-12 LBD with mammalian nuclear receptor LBDs. Interestingly, DAF-12 shares specific structural features with the mammalian bile acid receptor FXR, especially with respect to the orientation of the bound ligand. This result suggests that their ligand binding mechanism and bile acid-like signaling pathways have been conserved across evolution. Finally we showed that bile acid(-like) metabolites in mammals can activate nematode DAF-12s and presented the crystal structure of the hookworm *Ace*DAF-12 LBD bound to (25S)-cholestenoic acid. Together, our work reveals the structural mechanism of ligand recognition by DAF-12 and

points to the basis for evolution of a novel gut parasite hormone signaling pathway.

EXPERIMENTAL PROCEDURES

Plasmids and Reagents—The mutants used for crystallization, AlphaScreen, or cotransfection assays were created by site-directed mutagenesis using the QuikChange method (Stratagene) and verified by sequencing. DAs and cholestenoic acids were synthesized as described elsewhere (1, 16).

Protein Preparation and Crystallization—DAF-12s were cloned as described and inserted as His_6-GST fusions into an engineered pET24 vector (14). For biochemical assays, the proteins were expressed in BL21 (DE3) cells and purified by glutathione-Sepharose chromatography, and their ligand binding activity was tested in AlphaScreen luminescence proximity assays (17). For crystallography, *Ace*DAF-12 LBD was expressed in BL21 (DE3) cells as His_6-SUMO fusion. The protein was first purified by nickel-nitrilotriacetic acid chromatography. The SUMO tag was removed with Ulp1 protease (18), and the untagged monomeric LBD was purified by size exclusion chromatography.

The purified *Ace*DAF-12 LBD protein was mixed with coactivator peptide (SRC2-3) and ligands ((25S)-Δ7-DA or (25S)-cholestenoic acid) for crystallization. The molar ratio of these components was 1 (DAF-12 protein):1.5 (peptide):5 (ligand). (25S)-Δ7-DA crystals were grown at 20 °C in sitting drops containing 1.0 μl of the protein solution (8.0 mg/ml) and 1.0 μl of the well solution containing 0.1 M sodium acetate, pH 5.1, 0.2 M ammonium acetate, 26% w/v PEG2000. (25S)-Cholestenoic crystals were grown at 20 °C in sitting drops containing 1.0 μl of the protein solution (7.3 mg/ml) and 1.0 μl of the well solution containing 0.2 M di-ammonium tartrate, 20% w/v PEG3350. In general, crystals appeared within 2 days and grew to the final size in about 1 week, at which time they were flash-frozen and stored in liquid nitrogen.

Data Collection, Structure Determination, Refinement, and Superposition—The diffraction data were collected with a MAR225 CCD detector at 21-ID beamline at the Advanced Photon Source at Argonne National Laboratory (Argonne, IL). The observed reflections were reduced, merged, and scaled with DENZO and SCALEPACK in the HKL2000 package. The structure was determined with the PHASER program by molecular replacement using the crystal structure of *Sst*DAF-12 as a model. Manual model building was carried out with the programs O (19) and QUANTA (Accelrys, Inc.), and the structure was refined with crystallography NMR software and CCP4 programs refmac5. Protein model superposition was performed using O. The data collection and structure determination statistics are summarized in Table 1.

AlphaScreen Assays—The binding of the cofactor motifs to DAF-12 LBDs was determined by AlphaScreen luminescence proximity assays as described (14, 17, 20). Reaction mixtures consisted of 50 nM His_6-GST fusion proteins, 20 nM biotinylated peptides, ligands (1 μM (25S)-Δ4- or (25S)-Δ7-DA or 10 μM (25S)- or (25R)-cholestenoic acid) or no ligand, 5 μg/ml nickel chelate-coated acceptor beads (PerkinElmer Life Sciences), and 5 μg/ml streptavidin-coated donor beads (PerkinElmer Life Sciences) in a buffer containing 50 mM

TABLE 1
Data collection and refinement statistics

	*Ace*DAF-12/(25*S*)-Δ7-DA	*Ace*DAF-12/(25*S*)-cholestenoic acid
PDB code	3UP0	3UP3
Data collection		
Space group	P21	P21
Resolution	50 to 1.60 Å	30 to 1.25 Å
Cell parameters *a*, *b*, and *c*	48.0, 85.1, 66.1 Å	34.5, 85.3, 46.3 Å
β	107.1°	106.9°
Unique reflections	67,306 (6745)	64,400 (4035)
R_{sym}	0.102 (0.609)	0.048 (0.400)
I/σ	22.0 (2.7)	35.2 (3.5)
Completeness	100% (100%)	91.2% (57.3%)
Redundancy	7.6 (7.5)	4.2 (3.8)
Structure determination and refinement		
Resolution	30 to 1.60 Å	30 to 1.25 Å
No. of reflections	57,044	59,703
No. of residues	509	261
No. of solvent molecules	543	224
No. of non-H atoms	4697	2326
R_{work}	18.34%	16.61%
R_{free}	20.19%	18.04%
r.m.s.d. bonds	0.013 Å	0.013 Å
r.m.s.d. angles	1.363°	1.522°
Average *B* factor,	14.402 Å^2	9.299 Å^2

MOPS, pH 7.4, 50 mM NaF, 50 mM CHAPS, and 0.1 mg/ml bovine serum albumin. The peptides used in our studies are listed in supplemental Table S1.

Cotransfection Assays—HEK293 and COS7 cells were cultured and cotransfected in 96-well plates as reported (14, 21). 15 ng of the coactivator SRC2 was coexpressed with *Sst*DAF-12 in Figs. 3*B* and 5*A* to increase the transfection signal. The same amount of SRC2 was coexpressed with *Ace*DAF-12 and *Cel*DAF-12 in Fig. 5*B*.

Hookworm Rescue Experiments—(25*S*)- or (25*R*)-cholestenoic acid in the indicated concentrations was tested for their ability to stimulate feeding in infectious *A. caninum* L3 larvae (*n* = 150). Experiments were conducted as described previously (14). Incubation at host-like temperature (37 °C) in medium supplemented with 15 mM *S*-methylglutathione and 10% canine serum filtrate is known to stimulate feeding of ~95% and was used as a positive control (supplemental Fig. S5*A*) (22).
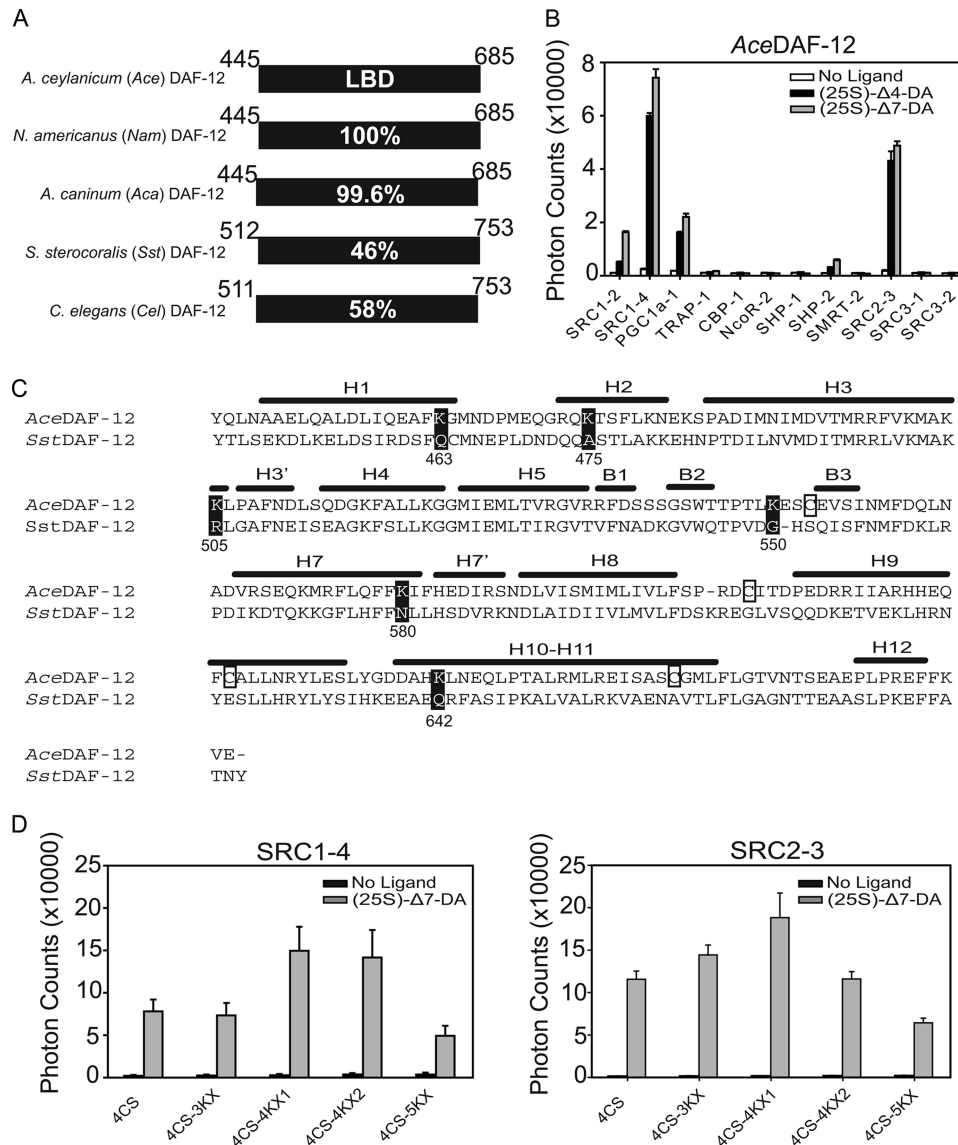
RESULTS

Crystallization of the A. ceylanicum DAF-12 LBD Complexed with (25S)-Δ7-DA—Sequence analysis revealed that hookworm DAF-12 LBDs are nearly 100% identical among *A. ceylanicum*, *N. americanus*, and *A. caninum* species but only share 46% sequence identity to the threadworm *Sst*DAF-12 LBD (Fig. 1*A*). In this study, we chose the *Ace/Nam*DAF-12 LBD (the *A. ceylanicum* and *N. americanus* LBDs are identical) for crystallization, because *A. ceylanicum* and *N. americanus* are the major cause for human hookworm infections (10). Reportedly, crystallization of a number of nuclear receptor LBD complexes requires the inclusion of L*XX*LL motifs (14, 17, 20). By doing so, the L*XX*LL motifs stabilize the AF2 helix (H12) that is otherwise relatively mobile and thus promote nuclear receptor crystal packing. Because the L*XX*LL-containing cofactors in *C. elegans* remain uncharacterized, we tested 12 mammalian L*XX*LL-containing coactivator peptides and L*XXX*I*XXX*(L/I)-containing corepressor peptides (see supplemental Table S1) for ligand-dependent *Ace*DAF-12 LBD interactions in AlphaScreen assays. As shown in Fig. 1*B*, *Ace*DAF-12 showed

strong binding to SRC1–4 and SRC2-3, in comparison with weaker binding to SRC1−2 and PGC1α-1 and in the presence of DAs. DAF-12 from *A. caninum*, *N. americanus*, and *S. stercoralis* species had similar binding patterns in the assays (supplemental Fig. S1). Accordingly, SRC1–4 and SRC2-3 peptides were included in our crystallization trials along with (25*S*)-Δ7-DA.

Initial attempts to express the *Ace*DAF-12 LBD yielded low amounts of soluble protein. Because cysteine mutation is a widely used strategy to solubilize recombinant proteins by preventing the random formation of disulfide bonds that cause protein precipitation (23), we mutated the four cysteines in the *Ace*DAF-12 LBD to serines (Cys → Ser). Evaluation of the predicted positions of these cysteine residues based on the *Sst*DAF-12 LBD structure suggested that these cysteines are distributed in loops or kinks, away from the functional cores (Fig. 1*C*). Mutation of four cysteines (4CS, C553S/C607S/C625S/C661S) markedly increased *Ace*DAF-12 LBD solubility and yielded 3– 4 mg of protein from 6 liters of culture, making crystallization possible. To facilitate crystallization, we also mutated a number of nonconserved lysines in *Ace*DAF-12 corresponding to surface amino acids in *Sst*DAF-12 that might affect crystal packing because of the flexibility of the lysine side chain (Lys → Xaa) (Fig. 1*C*). As a result, several *Ace*DAF-12 LBD mutants were made and used for crystallization. They were named *Ace*DAF-12 LBD 4CS-3KX (K475A/K505R/K550G plus 4CS), 4CS-4KX1 (K475A/K505R/K550G/K642Q plus 4CS), 4CS-4KX2 (K463Q/K475A/K505R/K550G plus 4CS), and 4CS-5KX (K475A/K505R/K550G/K580N/K642Q plus 4CS). 4CS-4KX1 yielded acceptable crystals for structure determination. Interestingly, these crystals could only be grown by using the sitting drop but not hanging drop technique under the same precipitation conditions. Notably, as predicted from the *Sst*DAF-12 LBD structure, Cys → Ser and Lys → Xaa mutations did not affect the ability of *Ace*DAF-12 to bind cofactor peptides in a DA-dependent manner in AlphaScreen assays (Fig. 1*D*).

A

A. ceylanicum (Ace) DAF-12   445   LBD   685

N. americanus (Nam) DAF-12   445   100%   685

A. caninum (Aca) DAF-12   445   99.6%   685

S. sterocoralis (Sst) DAF-12   512   46%   753

C. elegans (Cel) DAF-12   511   58%   753

B

*Ace*DAF-12

(Bar graph; y-axis: Photon Counts (x10000), 0–8; Legend: No Ligand, (25S)-Δ4-DA, (25S)-Δ7-DA; x-axis categories: SRC1-2, SRC1-4, PGC1a-1, TRAP-1, CBP-1, NcoR-2, SHP-1, SHP-2, SMRT-2, SRC2-3, SRC3-1, SRC3-2)

C

```
                              H1                             H2                          H3
AceDAF-12   YQLNAAELQALDLIQEAFKGMNDPMEQGRQKTSFLKNEKSPADIMNIMDVTMRRFVKMAK
SstDAF-12   YTLSEKDLKELDSIRDSFQCMNEPLDNDQQASTLAKKEHNPTDILNVMDITMRRLVKMAK
                              463                            475
              H3'       H4                      H5      B1      B2            B3
AceDAF-12   KLPAFNDLSQDGKFALLKGGMIEMLTVRGVRRFDSSSGSWTTPTLKESCEVSINMFDQLN
SstDAF-12   RLGAFNEISEAGKFSLLKGGMIEMLTIRGVTVFNADKGVWQTPVDG-HSQISFNMFDKLR
            505                                           550
                  H7           H7'        H8                            H9
AceDAF-12   ADVRSEQKMRFLQFFKIFHEDIRSNDLVISMIMLIVLFSP-RDCITDPEDRRIIARHHEQ
SstDAF-12   PDIKDTQKKGFLHFFNLLHSDVRKNDLAIDIIVLMVLFDSKREGLVSQQDKETVEKLHRN
                           580
                                    H10-H11                              H12
AceDAF-12   FCALLNRYLESLYGDDAHKLNEQLPTALRMLREISASCGMLFLGTVNTSEAEPLPREFFK
SstDAF-12   YESLLHRYLYSIHKEEABQRFASIPKALVALRKVAENAVTLFLGAGNTTEAASLPKEFFA
                           642
AceDAF-12   VE-
SstDAF-12   TNY
```

D

SRC1-4

(Bar graph; y-axis: Photon Counts (x10000), 0–25; Legend: No Ligand, (25S)-Δ7-DA; x-axis categories: 4CS, 4CS-3KX, 4CS-4KX1, 4CS-4KX2, 4CS-5KX)

SRC2-3

(Bar graph; y-axis: Photon Counts (x10000), 0–25; Legend: No Ligand, (25S)-Δ7-DA; x-axis categories: 4CS, 4CS-3KX, 4CS-4KX1, 4CS-4KX2, 4CS-5KX)

FIGURE 1. **Strategy for crystallization of the *Ace*DAF-12 LBD.** *A,* sequence identity of DAF-12 homologs from parasitic nematodes. *Numbers* refer to the amino acid position in the LBD of each receptor. Amino acid 449 is alanine in *Ace*DAF-12 and *Nam*DAF-12 but is valine in AcaDAF-12. *B,* AlphaScreen assays to search for *Ace*DAF-12-interacting peptides. 1 μm (25*S*)-DA is used. *C,* alignment of secondary structural elements of the *Ace*DAF-12 LBD is based on the crystal structure of the *Sst*DAF-12 LBD. H, α-helix; *B,* β-strand. Cysteines in *Ace*DAF-12 that were mutated to serines are *boxed*. Lysines in *Ace*DAF-12 that were mutated to the corresponding amino acids in *Sst*DAF-12 are highlighted in *black*. *Numbers* refer to the lysine position in the *Ace*DAF-12 LBD. *D,* ligand binding function of *Ace*DAF-12 mutants for crystallization is examined in AlphaScreen assays. 4CS, C553S/C607S/C625S/C661S; 4CS-3KX, K475A/K505R/K550G plus 4CS; 4CS-4KX1, K475A/K505R/K550G/K642Q plus 4CS; 4CS-4KX2, K463Q/K475A/K505R/K550G plus 4CS; 4CS-5KX, K475A/K505R/K550G/K580N/K642Q plus 4CS. 1 μm (25*S*)-DA is used. 4CS-4KX1 was successful for subsequent crystallization.

Structure Analysis of the AceDAF-12 LBD Complexed with (25S)-Δ7-DA—The *Ace*DAF-12 LBD/(25*S*)-Δ7-DA structure was solved at a resolution of 1.60 Å, with two complexes, herein referred to as *a* and *b*, each in noncrystallographic symmetric unit. The overall architecture of both complexes is similar to other nuclear receptor LBDs, appearing as a well wrapped three layer α-helical sandwich made of 13 α-helices and 3 β-strands (Fig. 2*A* shows complex *a*). The ligand is surrounded by the same sets of amino acids in both complexes as seen in the structure of the threadworm *Sst*DAF-12 LBD (14), consisting of hydrophobic amino acids surrounding the steroid skeleton and polar amino acids interacting with both ends of the ligand (Fig. 2*B* and supplemental Fig. S2). Superposition of *a* and *b* complexes indicates that they have a root

mean square deviation (r.m.s.d.) of 0.563 Å. The major difference between the two complexes is the conformation of β-turns, which causes the ligand ((25*S*)-Δ7-DA) to take a slightly different conformation in the ligand binding pocket because of the differential space arrangements of the ligand in the two complexes. The C3-keto group of Δ7-DA forms an H-bond with Gln-571 in *b* (3.1 Å), which is absent in *a*. Instead, Δ7-DA forms a single H-bond with a nearby water molecule (2.8 Å) in *a*, an interaction also witnessed in *b* (3.3 Å) (Fig. 2*C*). There is also a difference in the length of H-bonds formed with the C27-carboxyl group of Δ7-DA in the two complexes (Fig. 2*D*). This finding suggests that *Ace*DAF-12 LBD may bind Δ7-DA in two slightly different modes, which are interconvertible in solution.
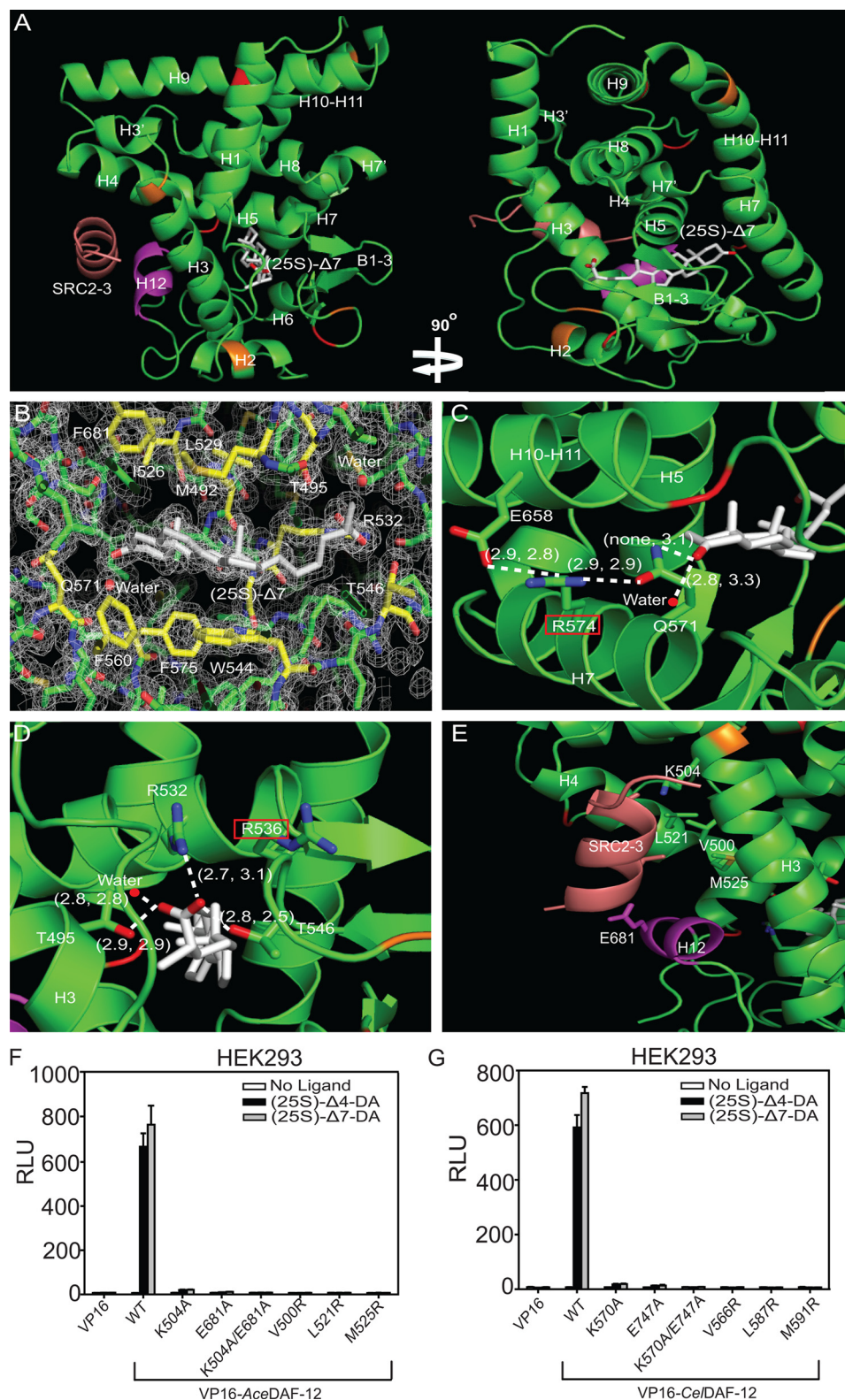
FIGURE 2. **Structure analysis of the *Ace*DAF-12 LBD.** *A, ribbon* model reveals the overall architecture of the *Ace*DAF-12 LBD chain *a* (*green*) complexed with (25*S*)-Δ7-DA (*white*) and the coactivator peptide SRC2-3 (*brown*). The AF-2 helix is highlighted in *magenta*. Mutated cysteines are in *red* and mutated lysines in *orange*. *B,* electron density map of the *Ace*DAF-12 *a* chain ligand binding pocket bound to (25*S*)-Δ7-DA. The surrounding amino acids are highlighted in *yellow*. See supplemental Fig. S2 for the electron density map of complex *b*. *C,* H-bonding of *Ace*DAF-12 amino acids and water involved in binding the C3-keto group of (25*S*)-Δ7-DA. Arg-574 (*red box*) serves as the H-bonding network hub. *D,* H-bonding of *Ace*DAF-12 amino acids and water to the C27-carboxyl group of (25*S*)-Δ7-DA. Arg-536 (*red box*) can compensate Arg-532 for interacting with the ligand. H-bonds are illustrated by *white dashed lines* with bond lengths noted in Å. The first number in *parentheses* indicates the bond length in complex *a* and the second number indicates bond length in complex *b*. *E,* amino acids involved in binding the coactivator peptide SRC2-3 (*salmon*) are labeled. *F* and *G,* mutation of the labeled amino acids (*E*) in *Ace*DAF-12 (*F*) or corresponding amino acids in *Cel*DAF-12 (*G*) disrupts the binding to SRC2-3 L*XX*LL coactivator motifs in mammalian two-hybrid assays performed in HEK293 cells. 1 μM (25*S*)-DA is used. *RLU* is relative light unit that is normalized with β-galactosidase activity as transfection control.
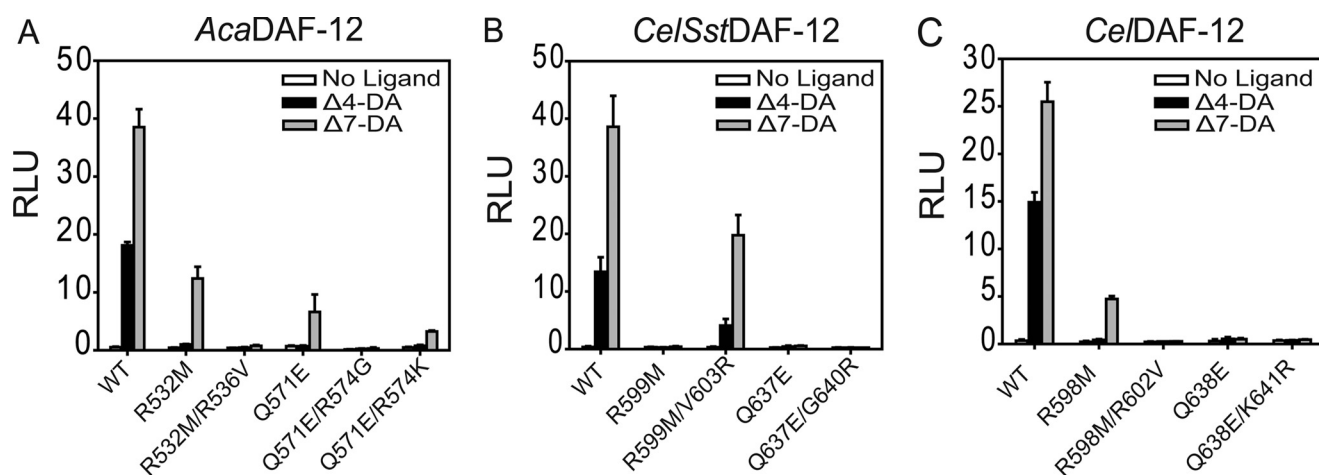
FIGURE 3. **Structural understanding of DAF-12 species-specific ligand binding.** *A–C*, site-directed mutagenesis validates the structural elements responsible for species-specific ligand binding, as revealed by structural comparison between *Ace*DAF-12 and *Sst*DAF-12 LBDs. Cotransfection assays are performed in COS7 cells. 1 μM (25*S*)-DA is used. *RLU*, relative light unit. *CelSst*DAF12, a hybrid between the N terminus of *Cel*DAF-12 and the LBD of *Sst*DAF-12. We used this chimeric construct because full-length *Sst*DAF-12 expresses poorly in mammalian cells (14).

*Ace*DAF-12 binds to the coactivator peptide (SRC2-3) in a manner reminiscent of other activated nuclear receptors. Fig. 2*E* shows that helix H12 is in its active conformation and packed against helices H3–H5 to form a functional coactivator binding surface. Lys-504 from the C-terminal end of helix H3 and Glu-681 from the center of the AF2 helix form the charge clamp that anchors both ends of the SRC2-3 peptide by H-bonding. The locked SRC2-3 peptide adopts a two-turn α-helical conformation and sticks to the binding surface via hydrophobic interactions with Val-500, Leu-521, and Met-525. These charge clamp and hydrophobic amino acids are conserved in *Cel*DAF-12 and *Sst*DAF-12, implying that two species use the same mechanism for coactivator binding. Mutations in any of these amino acids greatly compromise the ability of *Ace*DAF-12 or *Cel*DAF-12 to recruit coactivators after ligand stimulation (Fig. 2, *F* and *G*).

Comparison of AceDAF-12 and SstDAF-12 LBD Structures— The DA complexes *a* and *b* have an overall architecture similar to the *Sst*DAF-12 LBD (complexed with (25*R*)-Δ7-DA), revealed by superposition (both r.m.s.d.s = 1.13). The only noticeable difference is the ligand conformation, which is probably due to the opposite stereochemistry at the C25 position of ligands (see supplemental Fig. S3). With two DAF-12 LBD structures, we first investigated why DAF-12 has species-specific responses to DAs (14).

It was previously shown that mutation of key ligand-binding residues (R532M/R599M/R598M and Q571E/Q637E/Q638E) differentially affected DA binding in hookworm, threadworm, and *C. elegans* DAF-12 (14). Our *Ace*DAF-12/(25*S*)-Δ7-DA structure reveals the molecular basis for these differences. At the C27-carboxyl end of Δ7-DA, Arg-536 of *Ace*DAF-12 is pointed away from the carboxyl group due to charge repulsion by Arg-532 (Fig. 2*D*). We reasoned that exchange of Arg-532 with a noncharged methionine is likely to allow the Arg-536 side chain to swing back and to replace Arg-532 in binding the ligand carboxyl group (Fig. 2*D*). The amino acid corresponding to Arg-536 in *Sst*DAF-12 is a valine (Val-603), which cannot compensate for a mutation of the Arg-532 analogous *Sst* Arg-599, making DA binding markedly more dependent on *Sst* Arg-

599 than on *Ace* Arg-532. However, this compensation is impaired in *Aca*DAF-12R532K and *Cel*DAF-12R598K (14) because the mutated lysine repels the charge of the compensating arginine, thereby preventing its H-bonding to the ligand. We confirmed this mechanism by introducing a R536V mutation in *Aca*DAF-12 R532M and a R602V mutation in *Cel*DAF-12 R599M, both of which abolished ligand activation of DAF-12 (Fig. 3, *A* and *C*). In contrast, the reciprocal mutation of V603R in *Sst*DAF-12R599M recovered the receptor activity (Fig. 3*B*).

At the other end of Δ7-DA is an H-bonding network based on Arg-574, which interacts with Gln-571 and Glu-658, respectively (Fig. 2*C*). This network increases the tolerance of hookworm DAF-12 against mutation of Gln-571, which locks the C3-keto group of the ligand by H-bonding (Fig. 2*C*). Correspondingly, *Ace*DAF-12 Q571E, but not *Cel*DAF-12Q638E or *Sst*DAF-12Q637E, can still be activated by Δ7-DA (14), because the H-bonding network hub Arg-574 still makes Glu an effective H-bond donor for the C3-keto group of Δ7-DA. The corresponding amino acids Gly-640 in *Sst*DAF-12 and Lys-641 in *Cel*DAF-12 cannot, or only weakly, form these H-bonding interactions. We confirmed this mechanism by introducing an R574G mutation into *Aca*DAF-12 Q571E, which as expected abolished the response of the receptor to Δ7-DA stimulation. Moreover, introduction of R574K that weakens the H-bonding network, partially impaired receptor activity (Fig. 3*A*). However, introduction of K641R into *Sst*DAF-12 Q637E or G640R into *Cel*DAF-12 Q638E did not rescue the receptor response to Δ7-DA (Fig. 3, *B* and *C*), suggesting the involvement of other structural elements in hookworm DAF-12s that assist in ligand binding. In addition, in both hookworm complexes *a* and *b*, a water molecule is located near either end of (25*S*)-Δ7-DA and H-bonds with the ligand, which is not seen in the *Sst*DAF-12 LBD structure (Fig. 2, *C* and *D*).

Comparison of AceDAF-12 and FXR LBD Structures—Primary sequence analysis of full-length nuclear receptors suggested that DAF-12 is most similar to mammalian FXR, LXR, constitutively active receptor, pregnane X receptor, and vitamin D receptor. The LBD of DAF-12 is 33% identical to that of
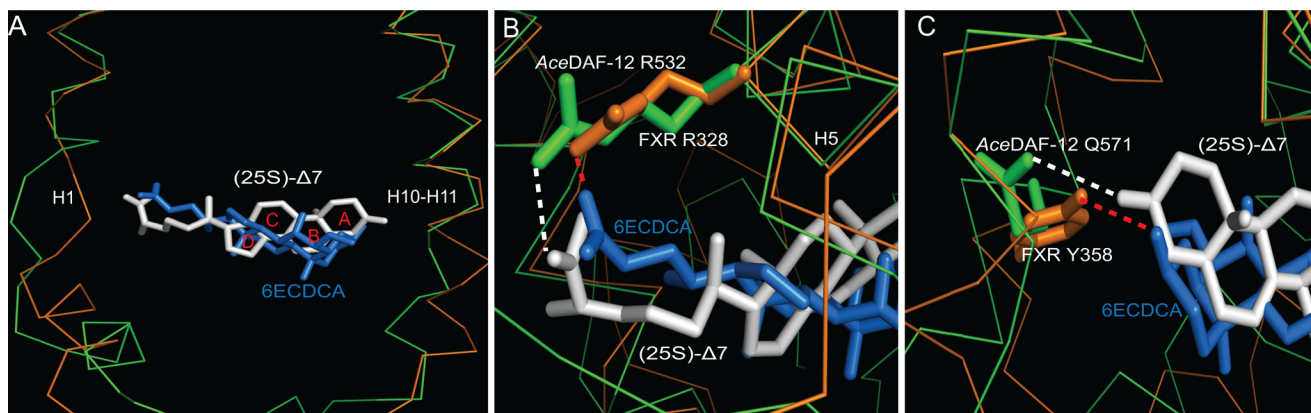
FIGURE 4. **Structural similarity between DAF-12 and FXR LBDs.** *A,* superposition of the *Ace*DAF-12 LBD complex *a* (*green*) onto the FXR LBD (*orange*). (25S)-Δ7-DA is in *white* and the FXR ligand 6ECDCA is in *blue*. The ligand orientation is the same in FXR and DAF-12 but different from that in other nuclear receptors. Rings of the Δ7-DA steroid skeleton are labeled as *A–D*. *B,* amino acids involved in binding the carboxyl group of the ligand are conserved. *C,* H-bond interactions with the C3 end of the ligand are similar. FXR Tyr-358 H-bonds with the C3-hydroxyl group of 6ECDCA (*red dashed line*), and *Ace*DAF-12 Gln-571 H-bonds with the C3-keto group of Δ7-DA (*white dashed line*) as seen in complex *b*.

FXR, 29% to LXRβ, 26% to LXRα, 26% to constitutively active receptor,, 25% to pregnane X receptor, and 23% to vitamin D receptor (5, 24). To understand the similarity between DAF-12 and mammalian nuclear receptors on a three-dimensional structural basis, we superposed the *Ace*DAF-12 LBD complex *a* onto a number of mammalian nuclear receptor LBD-ligand complexes. DAF-12 shares a closer three-dimensional structural appearance to FXR, LXR, and vitamin D receptor as predicted by the primary sequence analysis (The calculated r.m.s.d. are summarized in supplemental Table S2). Interestingly, further inspection revealed that DAF-12 and FXR adopt the same ligand orientation that is different from other nuclear receptors (25). Their A ring of the steroid skeleton faces the back layer of the ligand binding pocket in both DAF-12 and FXR, and their D ring faces outward toward helix H1 (Fig. 4*A*), whereas all other known nuclear receptors (including LXR and vitamin D receptor) arrange their cognate steroid-based ligands in the opposite direction (26, 27). Furthermore, DAF-12 and FXR use conserved amino acids to interact with the carboxyl group of the ligand. The interaction of *Ace*DAF-12 Arg-532 with the carboxyl group of Δ7-DA corresponds to the binding of FXR Arg-328 to the carboxyl group of its ligand 6α-ethyl-chenodeoxycholic acid (6ECDCA) (Fig. 4*B*). Although the amino acids are not conserved in binding the other end of the ligand, a similar H-bond interaction between Gln-571 and the C3-keto group of Δ7-DA in *Ace*DAF-12 also occurs with the corresponding amino acid Tyr-358 in FXR to form an H-bond with the C3-hydroxyl group of 6ECDCA (Fig. 4*C*). The three-dimensional structural similarity between DAF-12 and FXR indicates that they share common structural features in binding bile acid-like molecules and suggests that FXR is the closest DAF-12 ortholog among mammalian nuclear receptors.

Activation of AceDAF-12 by Mammalian Bile Acid(-like) Metabolites—DAs were identified in *C. elegans*, but so far they have not been detected in parasitic nematodes (1). Most parasitic nematodes constitutively enter iL3 and are unable to complete development outside their hosts, perhaps because of missing parts of the enzyme cascade that generates DAF-12 ligands (14). Consistently, the orthologs for DAF-9 (the key enzyme in *C. elegans* DA production) have not been characterized in par-

asitic nematodes. Also, the difference of EC_{50} values in DA activation of *C. elegans* and parasitic DAF-12s suggests that parasitic DAF-12s have their own distinct physiological ligands (14). The biosynthesis of bile acids and DAs has the same chemistry, and their binding to the receptors conserves the same structural mechanism. Therefore, we wanted to investigate what mammalian bile acid(-like) metabolites can activate the parasitic DAF-12s and be their potential host ligands.

Previous studies have showed that mammalian bile acid metabolites such as 3-keto LCA could activate *Cel*DAF-12 (1). In this study, we examined the effect of 3-keto LCA on parasitic DAF-12s from *S. stercoralis* and *A. caninum*. As shown in Fig. 5*A*, 3-keto LCA stimulated the activity of all the tested DAF-12s to a comparable level. However, 3-keto LCA is toxic at a higher concentration (28) and thus unlikely to be the host ligand.

Cholestenoic acid is a bile acid-like metabolite and circulates in human blood with concentrations between 300 and 500 nM (29). It is a potential product of 27-hydroxycholesterol by CYP27A1 action, whereas 27-hydroxycholesterol is a product of cholesterol by CYP27A1 action and serves as one of the bile acid precursors (3, 29). (25S)-Cholestenoic acid has been shown to weakly activate *Cel*DAF-12 and rescue the dauer formation in *daf-9* mutants (30). Therefore, we investigated the effect of this bile acid-like metabolite on the hookworm *Ace*DAF-12 activation together with its (25R)-diastereomer. The cotransfection assay results indicated that *Ace*DAF-12 was more sensitive to (25S)-cholestenoic acid ($EC_{50} = 4 \mu$M) than *Cel*DAF-12 ($EC_{50} > 30 \mu$M) (Fig. 5*B*), whereas *Cel*DAF-12 has the higher binding affinity to DAs than *Ace*DAF-12 (14). The activities of both DAF-12s were not stimulated by (25R)-cholestenoic acid, suggesting the importance of stereochemistry at the C25 position as previously shown (1, 30).

Structure of a Complex between the AceDAF-12 LBD with (25S)-Cholestenoic Acid—To understand the molecular basis for DAF-12 activation by mammalian bile acid(-like) metabolites, we set out to solve the x-ray crystal structure of the *Ace*DAF-12 LBD complexed with (25S)-cholestenoic acid. AlphaScreen interaction assays demonstrated that DAF-12s have a similar binding peptide profiling in the presence of cholestenoic acids relative to DAs (supplemental Fig. S4). Interest-
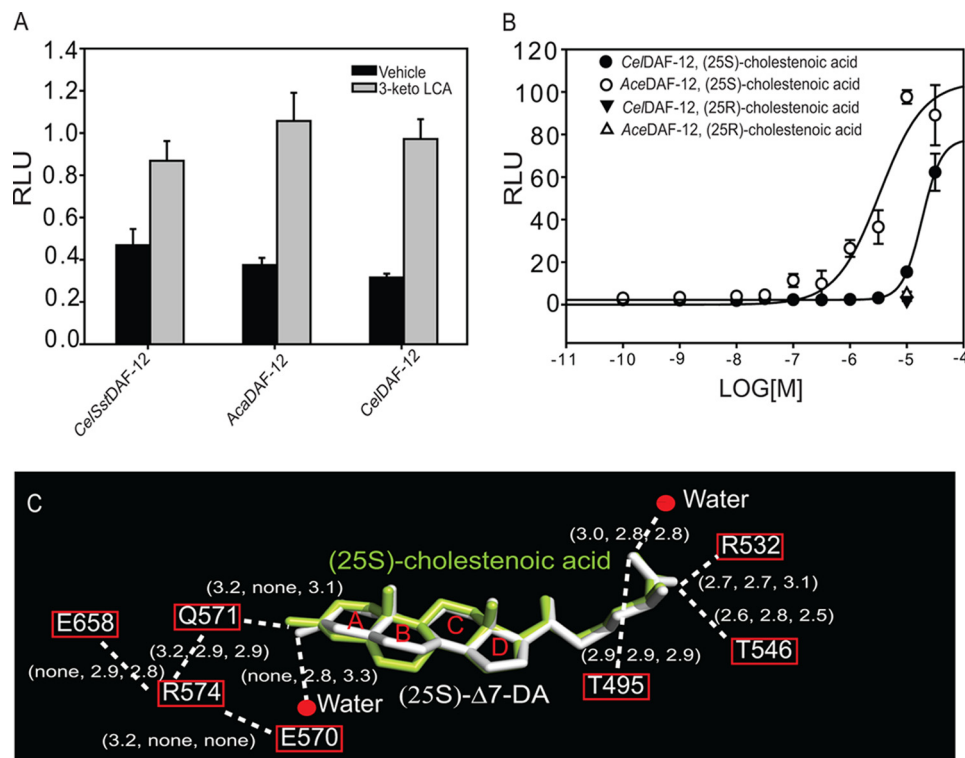
FIGURE 5. **Activation of DAF-12 by mammalian bile acid(-like) metabolites.** *A*, 3-keto LCA (10 μM) activates the DAF-12s from *S. stercoralis*, *A. caninum,* and *C. elegans* in COS7 cells. *B*, (25*S*)-cholestenoic acid activates the DAF-12s from *A. ceylanicum* and *C. elegans* in a dose-dependent manner in HEK293 cells. *RLU*, relative light unit. *C*, comparison of the H-bonding network involved in ligand binding in the *Ace*DAF-12 LBD-cholestenoic acid complex, DA complex *a*, and complex *b*. H-bonds are illustrated by *white dashed lines* with bond lengths noted in Å. The *1st number in parentheses* indicates the bond length in the cholestenoic acid complex. The *2nd* and *3rd number* indicate the bond length in the (25*S*)-DA complex *a* and *b*, respectively. Rings of the steroid skeleton are labeled as *A–D*.

ingly, both (25*S*)- and (25*R*)-cholestenoic acids can bind DAF-12s in AlphaScreen assays, suggesting that, *in vivo*, the physiological context of endogenous coactivators plays an important role in dictating activity.

The structure was determined at a high resolution of 1.25 Å. The electron density map precisely illustrated the amino acids and waters involved in binding the ligand (supplemental Fig. S5). Comparison of this structure to the DA complex *a* or *b* by superposition indicated a very close overlapping of the three-dimensional architectures (both r.m.s.d. = 0.437). The only noticeable difference lies in the conformation of the ligands that are well overlapped except for their A and B rings (Fig. 5*C*). This is caused by the double bond position on their B rings and results in different H-bonding networks at the C3-end of ligands. Structure analysis explains the weaker binding of cholestenoic acid to *Ace*DAF-12 relative to DA. First, the water molecule that forms H-bonds with the C3-end of the ligand in the (25*S*)-Δ7-DA structures is not present in the cholestenoic acid structure (see Figs. 5*C* and 2*C*). Second, all the H-bonds that build up the C3-end network are weaker in the cholestenoic acid structure. Interestingly, the network hub Arg-574 forms H-bonds with Glu-570, instead of interacting with Glu-658 as seen in the DA structure. Because the corresponding arginine is absent in *Cel*DAF-12 (Lys-641), a delicate H-bonding network that assists the ligand binding may not exist in *Cel*DAF-12. This difference can account for the much higher activity of (25*S*)-cholestenoic acid for *Ace*DAF-12 relative to *Cel*DAF12. Together, the configuration of the A and B rings is

the major determinant of ligand potency, as the ligand binding pattern is similar at the C27-carboxylic end of both ligands (see Figs. 5*C* and 2*D*).

DISCUSSION

In this paper, we present high resolution structures of two DAF-12 complexes that represent the first hookworm nuclear receptor structures. Our analysis reveals the structural features for the species-specific responses of DAF-12. This work also contributes to our understanding of the biochemical principles that may have guided the convergent evolution of a unique parasite-host relationship. In *C. elegans* DAs work as key postprandial signals through the nuclear receptor DAF-12 to direct worm energy utilization. This pathway is reminiscent of the function of bile acids in mammals to direct postprandial nutrient energy homeostasis through the nuclear receptor FXR (31). Indeed, the biochemistry of the DA-DAF-12 endocrine signaling pathway shares a remarkable similarity to that of the bile acid-FXR signaling pathway (Fig. 6). DA and bile acids are chemically similar steroid hormones that are synthesized by orthologous cytochrome P450 enzymes (DAF-9 and CYP27A1), and as shown in this study, DA and bile acids bind in a similar fashion to orthologous nuclear receptors (DAF-12 and FXR). Importantly, the DAF-12 pathway is also conserved in parasitic species (14, 15), with the intriguing exception that no parasite homologs of DAF-9 have been characterized to date. These findings imply that parasitic nematodes, unlike free-living *C. elegans*, may lack the ability to produce their own DAF-12
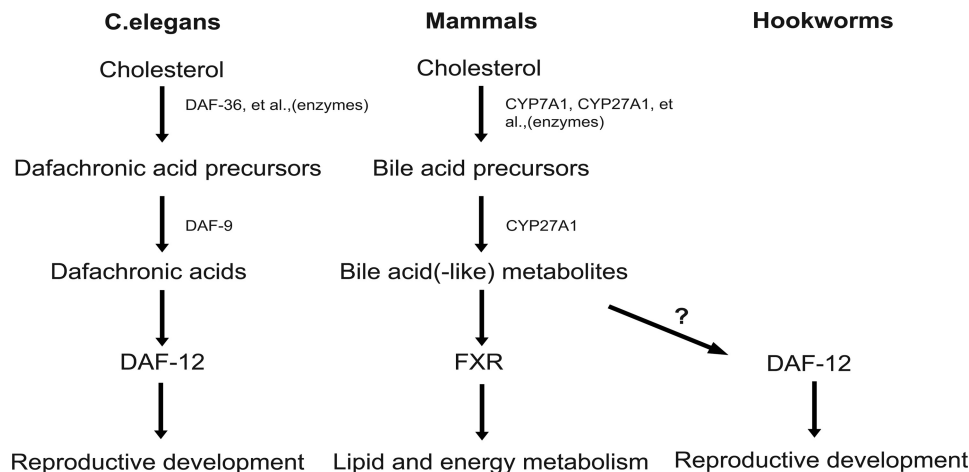
FIGURE 6. **Model of conserved bile acid-like signaling pathways in nematodes and mammals.** Bile acid-like signaling pathways in mammals and nematodes are compared and illustrated. Free-living nematodes (*e.g. C. elegans*) produce their own DAF-12 ligands to regulate the reproductive development. Parasitic nematode (*e.g.* hookworms) might use the host bile acid(-like) metabolites to activate their DAF-12 to regulate the reproductive development.

ligands. Thus, we propose a model in which infective iL3 worms, upon entering their host, are stimulated by specific bile acid-like hormones to begin their parasitic reproductive stage. This notion is supported further by our biochemical and structural studies showing mammalian bile acid metabolites can preferentially bind and activate the parasitic *versus C. elegans* DAF-12 receptor. In this scenario, the obligate enteric environment of parasitic worms might provide an abundant source of host-specific DAF-12 ligands. Our preliminary results showed that cholestenoic acids could not induce recovery of hookworm iL3 larvae (supplemental Fig. S6), and the identity of the physiological ligands that activate hookworm DAF-12 within the host remains the subject of future investigation.

The structures of the *Ace*DAF-12 LBD bound to (25*S*)-Δ7-DA and (25*S*)-cholestenoic acid not only illustrate the molecular mechanism for the interplay between parasite and host but also establish the structural framework for DAF-12 as a molecular target for treating nematode parasitism. This concept is strengthened by recent studies showing that DAF-12 is required for worms both to enter and exit the dauer diapause, which in parasites is the infectious stage. Thus, DAF-12 agonists might be used outside of the host to stimulate iL3 worms to prematurely molt into unviable L4 worms, whereas DAF-12 antagonists might be used within the host to prevent reproductive maturation (14, 15). Given the health importance of nematode parasites worldwide, the increasing prevalence of acquired drug resistance to current anthelmintics, and the lack of any drugs that target infectious stages (10, 32), these structural studies may provide key pharmacological insight into the potential design of species-specific ligands that target DAF-12.

REFERENCES

1. Motola, D. L., Cummins, C. L., Rottiers, V., Sharma, K. K., Li, T., Li, Y., Suino-Powell, K., Xu, H. E., Auchus, R. J., Antebi, A., and Mangelsdorf, D. J. (2006) Identification of ligands for DAF-12 that govern dauer formation and reproduction in *C. elegans*. *Cell* **124,** 1209–1223
2. Rottiers, V., Motola, D. L., Gerisch, B., Cummins, C. L., Nishiwaki, K., Mangelsdorf, D. J., and Antebi, A. (2006) Hormonal control of *C. elegans* dauer formation and life span by a Rieske-like oxygenase. *Dev. Cell* **10,** 473–482
3. Russell, D. W. (2003) The enzymes, regulation, and genetics of bile acid synthesis. *Annu. Rev. Biochem.* **72,** 137–174
4. Wollam, J., Magomedova, L., Magner, D. B., Shen, Y., Rottiers, V., Motola, D. L., Mangelsdorf, D. J., Cummins, C. L., and Antebi, A. (2011) The Rieske oxygenase DAF-36 functions as a cholesterol 7-desaturase in steroidogenic pathways governing longevity. *Aging Cell* **10,** 879–884
5. Antebi, A., Yeh, W. H., Tait, D., Hedgecock, E. M., and Riddle, D. L. (2000) daf-12 encodes a nuclear receptor that regulates the dauer diapause and developmental age in *C. elegans*. *Genes Dev.* **14,** 1512–1527
6. Hu, P. J. (2007) The *C. elegans* Research Community, doi/10.1895/wormbook.1.144.1, www.wormbook.org
7. Fielenbach, N., and Antebi, A. (2008) *C. elegans* dauer formation and the molecular basis of plasticity. *Genes Dev.* **22,** 2149–2165
8. Ludewig, A. H., Kober-Eisermann, C., Weitzel, C., Bethke, A., Neubert, K., Gerisch, B., Hutter, H., and Antebi, A. (2004) A novel nuclear receptor/coregulator complex controls *C. elegans* lipid metabolism, larval development, and aging. *Genes Dev.* **18,** 2120–2133
9. Jasmer, D. P., Goverse, A., and Smant, G. (2003) Parasitic nematode interactions with mammals and plants. *Annu. Rev. Phytopathol.* **41,** 245–270
10. Hotez, P. J., Bethony, J., Bottazzi, M. E., Brooker, S., Diemert, D., and Loukas, A. (2006) New technologies for the control of human hookworm infection. *Trends Parasitol.* **22,** 327–331
11. Viney, M. E. (2009) How did parasitic worms evolve? *BioEssays* **31,** 496–499
12. Dieterich, C., and Sommer, R. J. (2009) How to become a parasite. Lessons from the genomes of nematodes. *Trends Genet.* **25,** 203–209
13. Viney, M. E., Thompson, F. J., and Crook, M. (2005) TGF-β and the evolution of nematode parasitism. *Int. J. Parasitol.* **35,** 1473–1475
14. Wang, Z., Zhou, X. E., Motola, D. L., Gao, X., Suino-Powell, K., Conneely, A., Ogata, C., Sharma, K. K., Auchus, R. J., Lok, J. B., Hawdon, J. M., Kliewer, S. A., Xu, H. E., and Mangelsdorf, D. J. (2009) Identification of the nuclear receptor DAF-12 as a therapeutic target in parasitic nematodes. *Proc. Natl. Acad. Sci. U.S.A.* **106,** 9138–9143
15. Ogawa, A., Streit, A., Antebi, A., and Sommer, R. J. (2009) A conserved endocrine mechanism controls the formation of dauer and infective larvae in nematodes. *Curr. Biol.* **19,** 67–71

16. Sharma, K. K., Wang, Z., Motola, D. L., Cummins, C. L., Mangelsdorf, D. J., and Auchus, R. J. (2009) Synthesis and activity of dafachronic acid ligands for the *C. elegans* DAF-12 nuclear hormone receptor. *Mol. Endocrinol.* **23,** 640–648

17. Li, Y., Choi, M., Suino, K., Kovach, A., Daugherty, J., Kliewer, S. A., and Xu, H. E. (2005) Structural and biochemical basis for selective repression of the orphan nuclear receptor liver receptor homolog 1 by small heterodimer partner. *Proc. Natl. Acad. Sci. U.S.A.* **102,** 9505–9510

18. Mossessova, E., and Lima, C. D. (2000) Ulp1-SUMO crystal structure and genetic analysis reveal conserved interactions and a regulatory element essential for cell growth in yeast. *Mol. Cell* **5,** 865–876

19. Jones, T. A., Zou, J. Y., Cowan, S. W., and Kjeldgaard, M. (1991) Improved methods for building protein models in electron density maps and the location of errors in these models. *Acta Crystallogr. A* **47**, 110–119

20. Li, Y., Choi, M., Cavey, G., Daugherty, J., Suino, K., Kovach, A., Bingham, N. C., Kliewer, S. A., and Xu, H. E. (2005) Crystallographic identification and functional characterization of phospholipids as ligands for the orphan nuclear receptor steroidogenic factor-1. *Mol. Cell* **17,** 491–502

21. Shulman, A. I., Larson, C., Mangelsdorf, D. J., and Ranganathan, R. (2004) Structural determinants of allosteric ligand activation in RXR heterodimers. *Cell* **116,** 417–429

22. Hawdon, J. M., Volk, S. W., Rose, R., Pritchard, D. I., Behnke, J. M., and Schad, G. A. (1993) Observations on the feeding behavior of parasitic third-stage hookworm larvae. *Parasitology* **106**, 163–169

23. Krylova, I. N., Sablin, E. P., Moore, J., Xu, R. X., Waitt, G. M., MacKay, J. A., Juzumiene, D., Bynum, J. M., Madauss, K., Montana, V., Lebedeva, L., Suzawa, M., Williams, J. D., Williams, S. P., Guy, R. K., Thornton, J. W., Fletterick, R. J., Willson, T. M., and Ingraham, H. A. (2005) Structural analyses reveal phosphatidylinositols as ligands for the NR5 orphan receptors SF-1 and LRH-1. *Cell* **120,** 343–355

24. Mooijaart, S. P., Brandt, B. W., Baldal, E. A., Pijpe, J., Kuningas, M., Beek- man, M., Zwaan, B. J., Slagboom, P. E., Westendorp, R. G., and van Heemst, D. (2005) *C. elegans* DAF-12, nuclear hormone receptors and human longevity and disease at old age. *Ageing Res. Rev.* **4,** 351–371

25. Mi, L. Z., Devarakonda, S., Harp, J. M., Han, Q., Pellicciari, R., Willson, T. M., Khorasanizadeh, S., and Rastinejad, F. (2003) Structural basis for bile acid binding and activation of the nuclear receptor FXR. *Mol. Cell* **11,** 1093–1100

26. Williams, S., Bledsoe, R. K., Collins, J. L., Boggs, S., Lambert, M. H., Miller, A. B., Moore, J., McKee, D. D., Moore, L., Nichols, J., Parks, D., Watson, M., Wisely, B., and Willson, T. M. (2003) X-ray crystal structure of the liver X receptor β ligand binding domain. Regulation by a histidine-tryptophan switch. *J. Biol. Chem.* **278,** 27138–27143

27. Rochel, N., Wurtz, J. M., Mitschler, A., Klaholz, B., and Moras, D. (2000) The crystal structure of the nuclear receptor for vitamin D bound to its natural ligand. *Mol. Cell* **5,** 173–179

28. Martinez-Augustin, O., and Sanchez de Medina, F. (2008) Intestinal bile acid physiology and pathophysiology. *World J. Gastroenterol.* **14,** 5630–5640

29. Setchell, K. D., Schwarz, M., O'Connell, N. C., Lund, E. G., Davis, D. L., Lathe, R., Thompson, H. R., Weslie Tyson, R., Sokol, R. J., and Russell, D. W. (1998) Identification of a new inborn error in bile acid synthesis. Mutation of the oxysterol 7α-hydroxylase gene causes severe neonatal liver disease. *J. Clin. Invest.* **102,** 1690–1703

30. Held, J. M., White, M. P., Fisher, A. L., Gibson, B. W., Lithgow, G. J., and Gill, M. S. (2006) DAF-12-dependent rescue of dauer formation in *Caenorhabditis elegans* by (25S)-cholestenoic acid. *Aging Cell* **5,** 283–291

31. Modica, S., Gadaleta, R. M., and Moschetta, A. (2010) Deciphering the nuclear bile acid receptor FXR paradigm. *Nuclear Receptor Signal.* **8,** e005

32. Kaplan, R. M. (2004) Drug resistance in nematodes of veterinary importance. A status report. *Trends Parasitol.* **20,** 477–481